

The Use of Phased-Array Doppler Sonars near Shore

JEROME A. SMITH

Scripps Institution of Oceanography, University of California, San Diego, La Jolla, California

(Manuscript received 19 January 2001, in final form 3 July 2001)

ABSTRACT

Phased-array Doppler sonars (PADS) have been used to probe an area several hundred meters on a side with 8-m spatial resolution, sampling every second or less with under 2 cm s^{-1} rms velocity error per sample. Estimates from two systems were combined to produce horizontal velocity vectors. Here, concerns specific to use of PADS in shallow water are addressed. In particular, the shallower the water is, the larger the fraction of bottom backscatter, so the stronger the bias is toward zero Doppler shift in the estimates. First, direct comparisons are made with other current measurements made during the multi-investigator field experiment "SandyDuck," sponsored by the Office of Naval Research, which took place in the autumn of 1997 off the coast of Duck, North Carolina. The coherences between PADS and in situ current measurements are high, but the amplitude of the sonar response is generally low. To explore this further, a simplified model of wave shoaling is developed, permitting estimates of wave-frequency velocity variances from point measurements to be extrapolated over the whole field of view of PADS for comparison. The resulting time-space movies of sonar response are consistent with quasi-steady acoustic backscatter intensity from the bottom competing with a variable backscatter level from the water volume. The latter may arise, for example, from intermittent injection of bubbles by breaking waves, producing patches of high or low acoustic response that advect with the mean flow. Once this competition is calibrated via the surface wave variance comparison, instantaneous measured total backscatter intensities can be compared with an estimated bottom backscatter level (which is updated on a longer timescale, appropriate to evolution of the water depth or bottom roughness) to provide corrected sonar estimates over the region.

1. Introduction

The flows near shore are forced by waves and wind, with additional influences due to the larger-scale context (tides, outflow from inlets, shelf waves, etc.). The dynamics near shore also involve bathymetry, with wave refraction (Kaihatu and Kirby 1995; Kennedy et al. 2000; Lippmann et al. 1996; Raubenheimer et al. 1996), "channeling" of the mean flows (Shepard and Inman 1950), and the movement of sediment (Inman et al. 1971; Inman and Brush 1973; Shepard and Inman 1950). An understanding of the form and dynamics of these interactions near shore could lead to predictions of instabilities and rip currents (Allen et al. 1996; Bowen and Holman 1989; Oltman-Shay et al. 1989; Ozkan-Haller and Kirby 1999; Reniers et al. 1997; Slinn et al. 1998), of the net effects on horizontal mixing and diffusion (Inman et al. 1971), and of the feedback on morphological evolution and beach erosion (Holman 1995; Holman and Bowen 1982). The fluxes of momentum, vorticity, and mass (including sand, bubbles, nutrients, eggs, larvae, pollutants, etc.) across the nearshore region

are important in the larger-scale perspective, too. Useful parameterization of these fluxes could be viewed as important "output" from an understanding of the nearshore dynamics, as well as a good measure of how well the dynamics are understood.

A significant requirement for studying the nearshore system is an ability to observe both the incident waves and the underlying flow. Ideally, one would like to resolve gradients in wave-related quantities (mass flux, radiation stress; e.g., Longuet-Higgins and Stewart 1962, 1964; Longuet-Higgins 1970) over an area while simultaneously resolving the associated currents over a wide range of scales in time and space. Vorticity associated with the flow would be useful as both a diagnostic of the dynamics and a critical link to modeling. However, from a practical point of view, vorticity and flux gradients involve spatial derivatives, which are hard to extract from observations.

Acoustic techniques show promise for such extensive probing of the region near shore. For example, a study of "rip currents" was carried out with an earlier version of phased-array Doppler sonars (PADS; Smith and Largier 1995). "Blocking" by the bubble plumes left by plunging breakers was described for systems from 40 to 200 kHz (Smith 1993; Thorpe and Hall 1993) and appears to limit applicability to the region outside the

Corresponding author address: Jerome A. Smith, Marine Physical Laboratory, Scripps Institution of Oceanography, University of California, San Diego, La Jolla, CA 92093-0213.
E-mail: jasmith@ucsd.edu

break point of incoming surf. Influences of surf-generated bubbles on acoustic propagation (Farmer et al. 2001) and of bubble advection in the surf zone (Dahl 2001) and in rip currents (Caruthers et al. 1999; Vagle and Farmer 2001) have been described more recently. However, biasing of Doppler-based velocity estimates toward zero by bottom interference has not been quantitatively addressed previously.

A companion paper (Smith 2001, manuscript submitted to *J. Atmos. Oceanic Technol.*) describes the general use of high-frequency PADS to probe near-surface horizontal velocities over a continuous time-space segment extending hundreds of meters on a side and many hours in duration. Given the comprehensive measurement needs mentioned above, application of this technique in the nearshore region is compelling. Continuous coverage of waves and currents in space and time appears feasible, permitting estimation of the vertical component of vorticity of the nearshore currents, and of the divergence of the waves' "radiation stress" and mass flux (for example). Smith (2001) describes the essential technique and algorithms yielding quantitative estimates of errors and biases, including an objective technique for combining information from two (or more) systems to estimate horizontal vector velocities.

Here concerns specific to using high-frequency (~ 200 kHz) PADS in shallow water are addressed. There are several aspects of the nearshore environment that distinguish it acoustically from deep water: 1) The bottom backscatters sound that competes with the signal from scatterers in the water volume. The received signal attributable to bottom backscatter varies with water depth, and can also vary slowly in time (presumably as bottom roughness characteristics evolve). In general, this becomes significant when the wind and waves are weak, when few bubbles are generated. 2) Plunging breakers can produce a "wall" of bubbles so dense it is acoustically impenetrable (Smith 1993; Thorpe and Hall 1993). This limits the shoreward extent of measurements, confining the sample area to outside the active surf zone. 3) There are large variations in the scatterer content of the water, on scales of meters to tens of meters [e.g., water advecting offshore in rip currents that are full of bubbles from the surf zone (Smith and Largier 1995)]. 4) Advection of water from inlets can also lead to variations in stratification and in particle content of the water.

These issues are addressed through comparisons with data collected as part of "SandyDuck," a multi-investigator field experiment sponsored by the Office of Naval Research with assistance from the Army Corps of Engineers and the United States Geological Survey. Data in or near the field of view of a dual-PADS deployment were provided (see acknowledgments) as vertical profiles in 25-cm bins at one location (3-min average currents) and from current meters at many locations near bottom (0.5-s samples). The selection of comparisons and the interpretation of the results are guided by consideration of the underlying physics. In particular,

the predictable behavior of surface waves propagating on a nearly planar beach permits the comparisons to be extended over the whole area, and to the full time-space behavior of the response. The results indicate a relatively straightforward competition between bottom and volume backscatter.

2. Experimental setup

Two PADS were deployed as part of SandyDuck in September and October of 1997 at the Field Research Facility (FRF) of the U.S. Army Corps of Engineers. Looking shoreward from the 6-m depth contour, they probed a total area about 400 m along shore by 350 m across shore (Fig. 1). Over the smaller region probed by both systems, perhaps 200 m by 300 m, horizontal velocity vectors are fully resolved. In the outer corners, only one component is resolved; however, these one-component estimates still provide useful information, particularly concerning wave propagation.

The Doppler processing, error estimation, and method for combining information from two (or more) PADS is discussed in Smith (2001, manuscript submitted to *J. Atmos. Oceanic Technol.*). Briefly, the approach is similar to the use of dual-Doppler radars to map winds, but using sound and covering a smaller area with higher resolution. An acoustic signal is projected in a wide horizontal fan, radiating outward in the water from the instrument package and filling the water column in shallow water. The sound scatters off particles in the water (especially bubbles) and off the bottom. Some backscattered sound returns to the sonar, where the signal is received on an array, is beam formed into returns from various directions, and is analyzed for frequency shift versus direction and elapsed time since transmission. For direct-path transmission and return, the time delay since transmission translates to distance from the sonar. The frequency shift of the backscattered signal (Doppler shift) is proportional to the radial component of the velocity of scatterers at the sample volume. The systems discussed here were operated at 190- and 225-kHz center frequencies, with 11 repeats of two different 13-bit Barker codes to spread the signal over 15.6-kHz bandwidth ($64\text{-}\mu\text{s}$ "bits," sampled every $32\text{ }\mu\text{s}$; Pinkel and Smith 1992; Smith 2001, manuscript submitted to *J. Atmos. Oceanic Technol.*). The measurements are resolved to 7.6 m (range) by 6° (bearing), with new estimates produced every 0.75 s, pair-averaged to 1.5-s sample rate. The resulting velocity "radials" have rms error levels on the order of 1.5 cm s^{-1} (Smith 2001). By combining the radial velocities from two such devices located some 300 m apart (Fig. 1), both horizontal components of velocity can be estimated on a grid several hundred meters on a side.

Vertical location (elevation angle) is not resolved; the $\sim 22^\circ$ vertical beamwidth takes in the whole water column, and the effective location of the measurements is dictated by the centroid of scatterers. In the frequency range considered here (175–240 kHz), microbubbles are

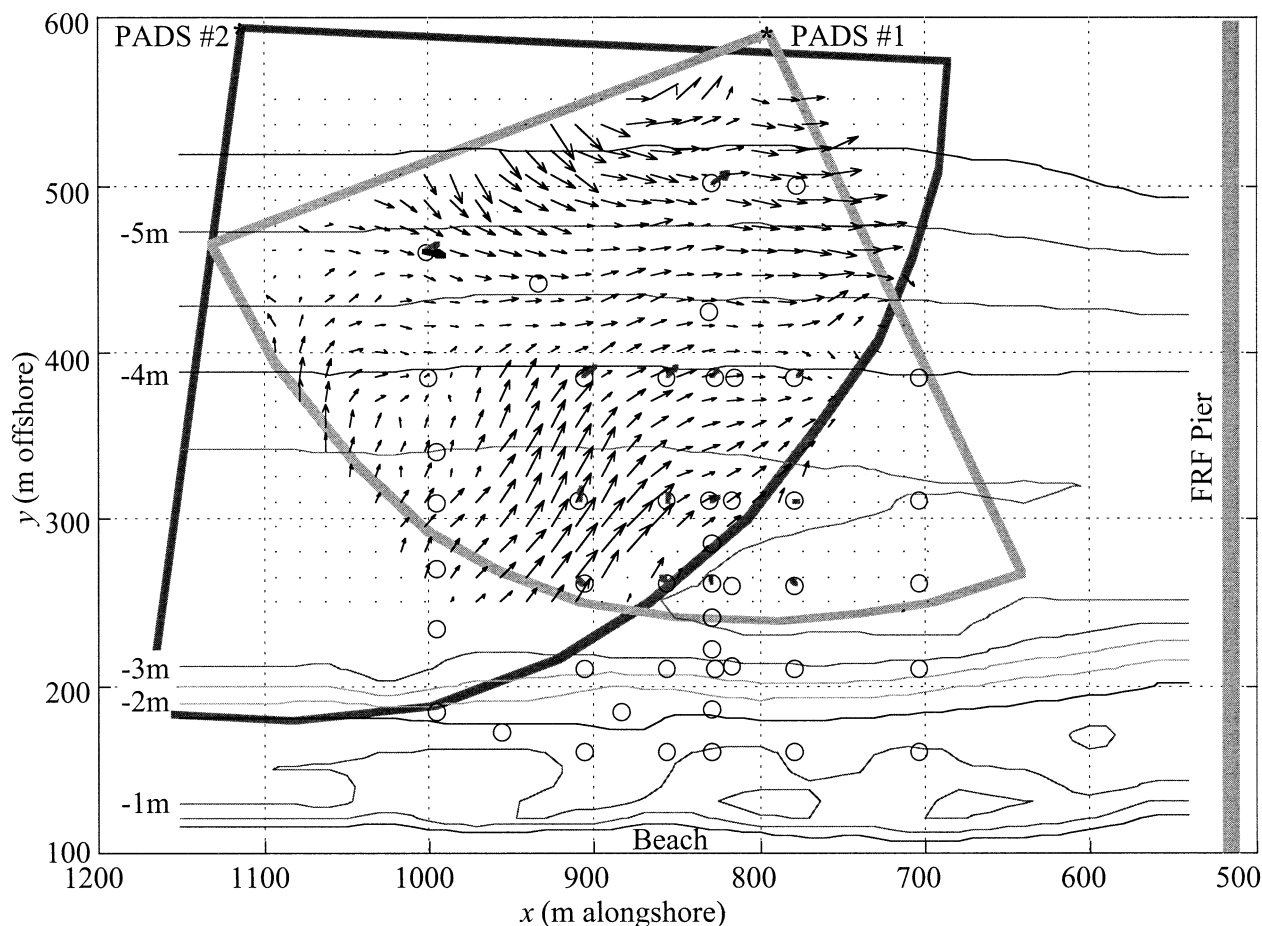


FIG. 1. SandyDuck experimental site, showing the area covered by the two PADS. The circles show locations of current measurements made by other investigators. The thin, dark arrows indicate velocity estimates from 2.5-min-averaged PADS data at 1640 UTC 13 Oct 1997, during stratified conditions. The longer arrows correspond to velocities near 12 cm s^{-1} . Vertical profiles are available at $x = 1000$, $y = 460$ (courtesy of P. Howd). The currents 1.5 m below the surface (thick, dark arrow) correspond closely to the PADS estimates. Currents closer to the bottom (thick, gray arrows centered in some of the circles) do not (see section 3a; other currents courtesy of S. Elgar, T. Herbers, W. O'Reilly, and R. Guza). North is about 20° clockwise of left. The location is the Field Research Facility of the U.S. Army Corps of Engineers, near Duck, NC.

efficient scatterers. These are produced copiously by breaking waves and, in general, dominate the backscatter even outside the surf zone when the wind exceeds 5 m s^{-1} or so (inside the surf zone, and in rip currents carrying surf-zone water offshore, microbubbles are ubiquitous). In deep water, bubble densities vary by orders of magnitude over moderate horizontal distances (depending strongly on wind speed) and have mean vertical distributions approximated by an exponential with a depth scale on the order of 1–2 m, depending weakly on wind speed (Crawford and Farmer 1987; Thorpe 1986). In shallow water this distribution may be different, and one issue here is the effective depth of the measurement.

3. Comparisons with current-meter data

a. Low-frequency comparisons

Recent studies with similar Doppler sonars used at grazing angles indicate that the velocity estimates cor-

respond to Eulerian velocities measured some depth below the wave troughs (Smith 1998). It is therefore appropriate to compare the low-frequency sonar estimates directly with those from current meters or profilers. This would also indicate that the low-frequency comparison is not sensitive to nonlinearity of the waves. The a priori hypothesis is that the effective depth of the sonar measurements is on the order of 1.5 m below the mean surface for typical oceanic conditions ($\sim 1\text{-m}$ waves, bubble layer with 1.5-m scale depth).

Comparisons are made first using velocities averaged over 1–5 min. For the resolved frequencies (low in comparison with the incident surface waves), stratification can be important. Thus, two time periods with contrasting conditions are examined: 1) 1600–1800 UTC 13 October 1997, a calm period with moderate stratification of the water column, and 2) 2100–2400 UTC 15 October 1997, a period with moderate winds and a well-mixed water column.

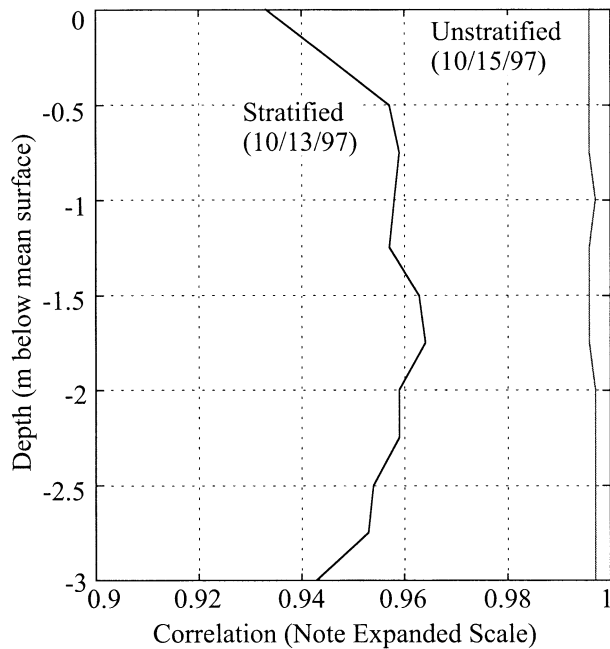


FIG. 2. Correlations between PADS data at the profile location and the horizontal currents measured at various depths. The stratified case (13 Oct 1997) exhibits a broad maximum near 1.5-m depth. The unstratified case (15 Oct 1997) yields higher correlations, with little if any depth dependence.

At one location, 3-min averaged current profiles were available. Figure 2 shows the correlations (means included) between PADS measurements versus the horizontal velocity at each depth, computed over the 2 h (on 13 October) or 3 h (15 October) of available data. In the stratified case (data from 13 October) the correlation varies with depth, providing one indication of the effective depth of the PADS measurements (not dissimilar to the a priori estimate). The well-mixed case (data from 15 October) shows better agreement between the PADS and currents at every depth measured (to 0.75 m from the bottom).

Comparisons were also made with data available from several other locations, but limited to current meters about 0.5 m off the bottom. For stratified cases, there can be substantial changes in current direction and mag-

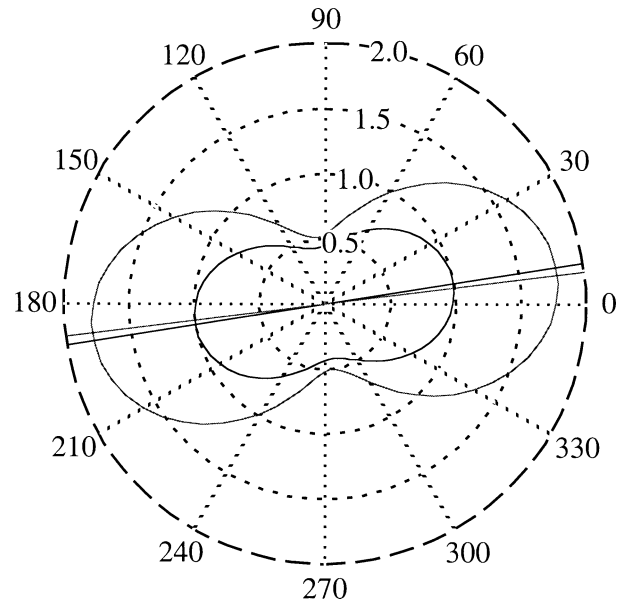


FIG. 3. Diagram illustrating the evolution of component velocity variance vs measurement angle between two depths. A directional distribution of 10.5-s-period waves is transformed from an initial position in 8-m water depth to 5-m depth using the simplified wave model (see text). Initial values (8-m depth): angle 9° , $H_s = 1.0$, $D = 0.70$ (inner, darker "pinched oval" with darker principal axis). At 5-m depth: angle 7.26° , $H_s = 1.6$, $D = 0.78$ (outer, lighter pinched oval with lighter principal axis).

nitude between the surface and bottom (see Fig. 1), and this situation can compromise comparisons made at these frequencies (low relative to surface-wave frequencies).

b. Wave-frequency correlations

To obviate effects of stratified flow, comparisons were made over the frequencies of the incoming waves. Suitable data, sampled at 2 Hz, were obtained from sonic altimeter, pressure, and cross-shore (U -) and alongshore (V -) current measurement frames (SPUVxx, where "xx" is an identification number). The SPUV current measurements are roughly 0.5 m above the bottom. In the comparison area (outside the surf zone), the depth

TABLE 1. Wave-frequency correlations and scale factors between PADS velocities and near-bottom current meters (SPUVs; see text). Locations are given in FRF coordinates (x increases offshore, shoreline is near 110 m; y increases along shore to the north-northwest; see Fig. 1). The magnitude of correlation between two SPUVs separated by 13 m (last column) is comparable to the correlation between the PADS and SPUV. Because of acoustic interference, PADS estimates from about 15 m away are used in the comparisons (see text). The scale factor required to bring PADS velocities up to the SPUV levels is always greater than 1. The systematic difference in scale between SPUV62 and SPUV63 may be due to undulations of the bottom or partial sheltering by the FRF pier (located 300 m to the south-southeast).

Run time	PADS/SPUV72 FRF $x, y = 500, 829$		PADS/SPUV62 $x, y = 385, 828$		SPUV62/SPUV63 $x = 385, y = 828$ vs 815	
	Correlation	Scale	Correlation	Scale	Correlation	Scale
1900 UTC 10 Sep 1997	0.939	1.13	0.925	1.46	0.907	0.976
0100 UTC 14 Oct 1997	0.873	1.65	0.725	3.73	0.890	0.935
0800 UTC 18 Oct 1997	0.936	1.59	0.855	1.75	0.865	0.943

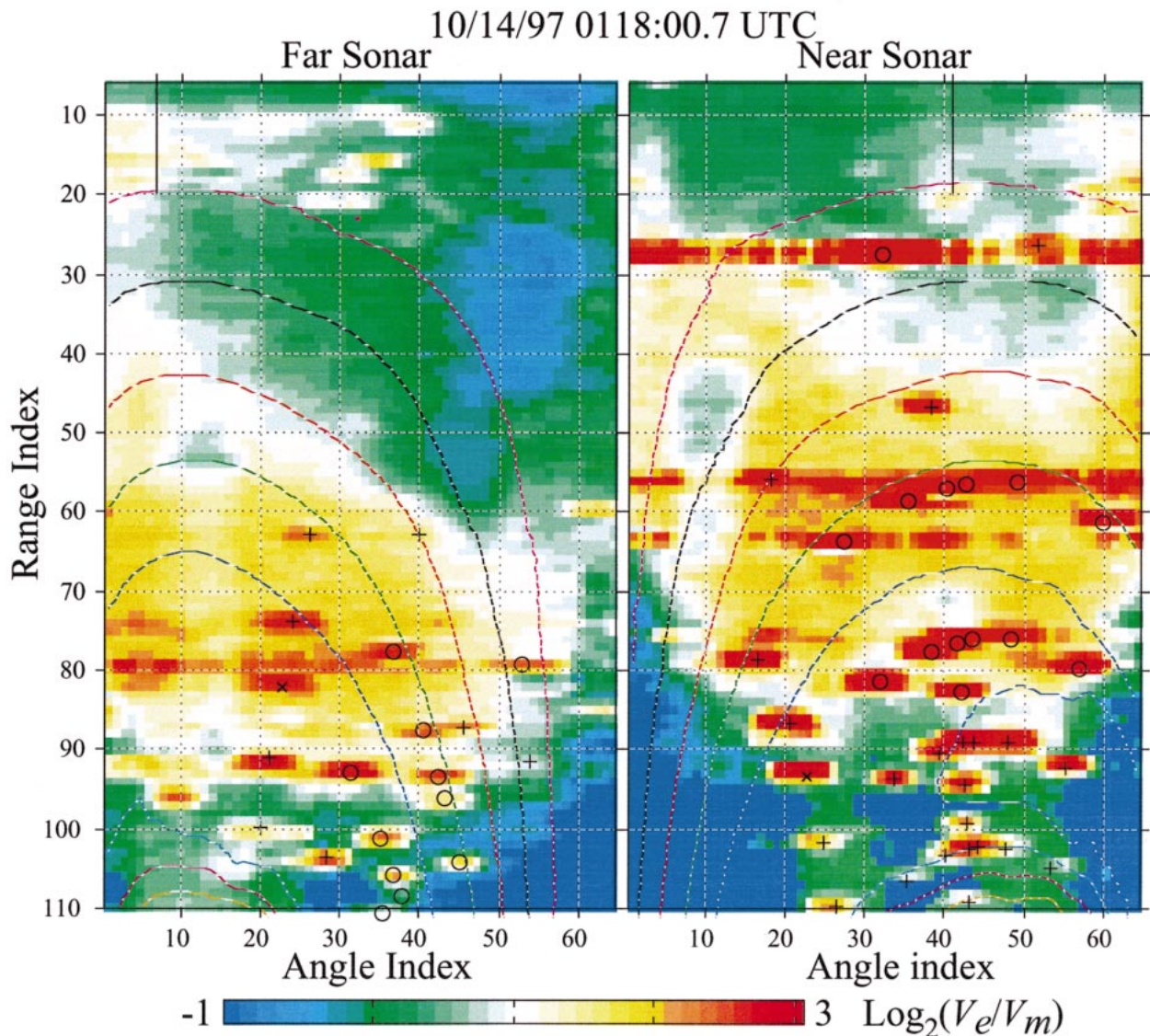


FIG. 4. Range-angle maps of the ratio of estimated rms wave orbital velocities parallel to the sonar beam (V_e) to measured rms values (V_m), for a day with low backscatter. The bottom contours illustrate the distortion due to viewing in range-angle coordinates (cf. Fig. 1). Green denotes equal variances, white denotes a measured variance of one-half the estimated value, tan means they are 1/4, and red means 1/8 or smaller. The lines extending upward from range index 20 in each panel denote the angle parallel to principal wave propagation direction. Over most of the areas covered by each sonar, the measured variances are systematically smaller than the estimated “true” values. The bias toward zero generally increases as the water depth decreases, until the signal fades at maximum range (near index 80–90). Backscatter from frames at the instrumented sites also reduces the measurement response. Range increments are 3.8 m, so the maximum range is about 418 m. Angle increments are 1.98° (far) and 1.76° (near), so the net angular spans are 128° (far sonar) and 113° (near sonar).

dependence of motion at wave frequencies is both moderate and well understood. Unfortunately, the support frames for the current meters produced significant acoustic interference. Fortunately, quantitative comparisons are usefully made between the current meter data and PADS estimates nearby (~ 15 m away), including both correlations and “scale factors” that relate the two kinds of data (see Table 1). These comparisons were carried out at 15 sites within the field of view of both PADS (see Fig. 1). The essence of the comparison is

demonstrated from a deeper site and two shallower sites (Table 1). It was found that the correlations between PADS velocities and the current meters are high, similar to those for similarly separated current meter pairs (Table 1, last column). However, while the correlations are high, the scaling factor relating the two kinds of data can vary from one run to another. The PADS estimates are systematically low; scaling factors up to 3.73 are needed to match the current meter magnitudes. Further, the scaling adjustment at the deeper site (Table 1, first

column) is always smaller than at shallower sites. This suggests that the cause may be interference from bottom backscatter (having zero or near-zero Doppler shift), which has increasing effect as the water depth decreases.

The correlations and scale factors were investigated as functions of frequency as well (cross-spectra and transfer functions). Within the limits of the resolved wave field, these appear to be uniform across frequency. This suggests that such wave-frequency comparisons can be used to “calibrate” the PADS estimates independent of frequency. However, we desire such a calibration over the whole field of view, not just at a few isolated points.

4. A simplified wave model

In this section a simple model is described for the evolution of waves as they shoal. Given values of wave properties at one or a few specified locations [e.g., from the SPUV arrays or at the 8-m array operated by C. Long of the FRF; see Long and Oltman-Shay (1991)], this model provides estimates of the radial velocity variances over the whole field of view of each PADS. For this purpose, the simplest description that captures the essence of the wave behavior is sought. Wave-frequency variances formed from averages over a few minutes from the PADS measurements can then be compared with the model-extrapolated estimates, providing statistical views of the sonar response as it evolves in time and space. The variances of velocity and elevation, and the relationships between them, are not sensitive to wave nonlinearity (in contrast to, e.g., skewness or asymmetry). Thus, a second-order description of the waves is adequate, which is a sufficient condition for action conservation to hold (Whitham 1974).

For a beach that is approximately uniform in the alongshore direction, the wave description reduces to a 1D problem, based on refraction, action conservation, and dissipation (Thornton and Guza 1986). Currents other than the orbital velocities of the waves are neglected. An adequate set of input parameters is provided by the depth profile $h(x)$ and wave properties at a specified depth (say at 8-m depth), for example, period T , a measure of wave amplitude such as significant wave height H_s , principal propagation direction φ , and a measure of the directional spread. The waves are assumed to be narrowband, so that a description based on the dominant period and direction is sufficient. In general, the mean wave propagation direction φ will tend toward the shoreline but be incident at some angle off normal (not quite parallel to the x axis, defined as shore-normal).

For waves that are statistically steady and homogeneous in y , action conservation reduces to

$$\frac{\partial}{\partial x}(c_x^g A) = 0, \quad (1)$$

where c_x^g is the x component of group velocity and A is the action density. Dissipation is neglected to simplify

exposition; however, it is straightforward to implement the semiempirical dissipation rate described by Thornton and Guza (1986), for example, and this was done for the data comparisons.

Wave action A is the ratio of wave energy to frequency, $A = E/\sigma$, where $E = \rho g H_s^2/32$. For statistically steady waves and no currents, the wave frequency $\sigma = 2\pi/T$ is constant. Gravity g and water density ρ are also constants, so A is simply proportional to H_s^2 . Thus, (1) integrates to

$$c_x^g H_s^2 = c^g H_s^2 \cos\varphi = \text{constant} \quad \text{or} \quad (2)$$

$$H_s^2(x) = H_0^2 \left[\frac{c_0^g \cos\varphi_0}{c^g(x) \cos\varphi(x)} \right], \quad (3)$$

where C_0^g , H_0 , and φ_0 are the values at the reference location.

To obtain c^g and φ as functions of x , first the wavenumber magnitude $k(x)$ is obtained (iteratively) from the linear dispersion relation for gravity waves in finite water depth,

$$\sigma^2 = gk \tanh kh, \quad (4)$$

given the frequency σ and water depth $h(x)$. The group speed is

$$c^g \equiv \frac{\partial \sigma}{\partial k} = \frac{1}{2} c^p \left[1 + \frac{2kh}{\sinh(2kh)} \right], \quad (5)$$

where $c^p \equiv \sigma/k$ is the phase speed. Since the system is uniform in y , conservation of wave crests implies that the y component of wavenumber k_y is constant (Phillips 1977). Then the propagation angle φ varies according to

$$\varphi = \arcsin \left[\left(\frac{k_0}{k} \right) \sin\varphi_0 \right], \quad (6)$$

where k_0 is the wavenumber at the reference location. Note that, particularly if the reference location is in shallower water than the target area, this can produce complex values. This implies an imaginary value of k_x , or an edge-wave-like solution. In the present context this does not cause problems.

The objective is to estimate velocity variances. It is instructive to consider a set of correlations between the Cartesian components of velocity in “beach coordinates,” $\langle V_x^2 \rangle$, $\langle V_y^2 \rangle$, and $\langle V_x V_y \rangle$, rather than wave height, direction, and directional spread (say). Here $\langle \rangle$ denote an appropriate average (e.g., over a few minutes). The principle wave direction can be found from the major axis of variability:

$$\varphi = \frac{1}{2} \arctan \left(\frac{2\langle V_x V_y \rangle}{\langle V_x^2 \rangle - \langle V_y^2 \rangle} \right). \quad (7)$$

The 180° ambiguity in direction hardly matters since the velocity variances are symmetric about wave propagation direction, but it is safe in this context to take

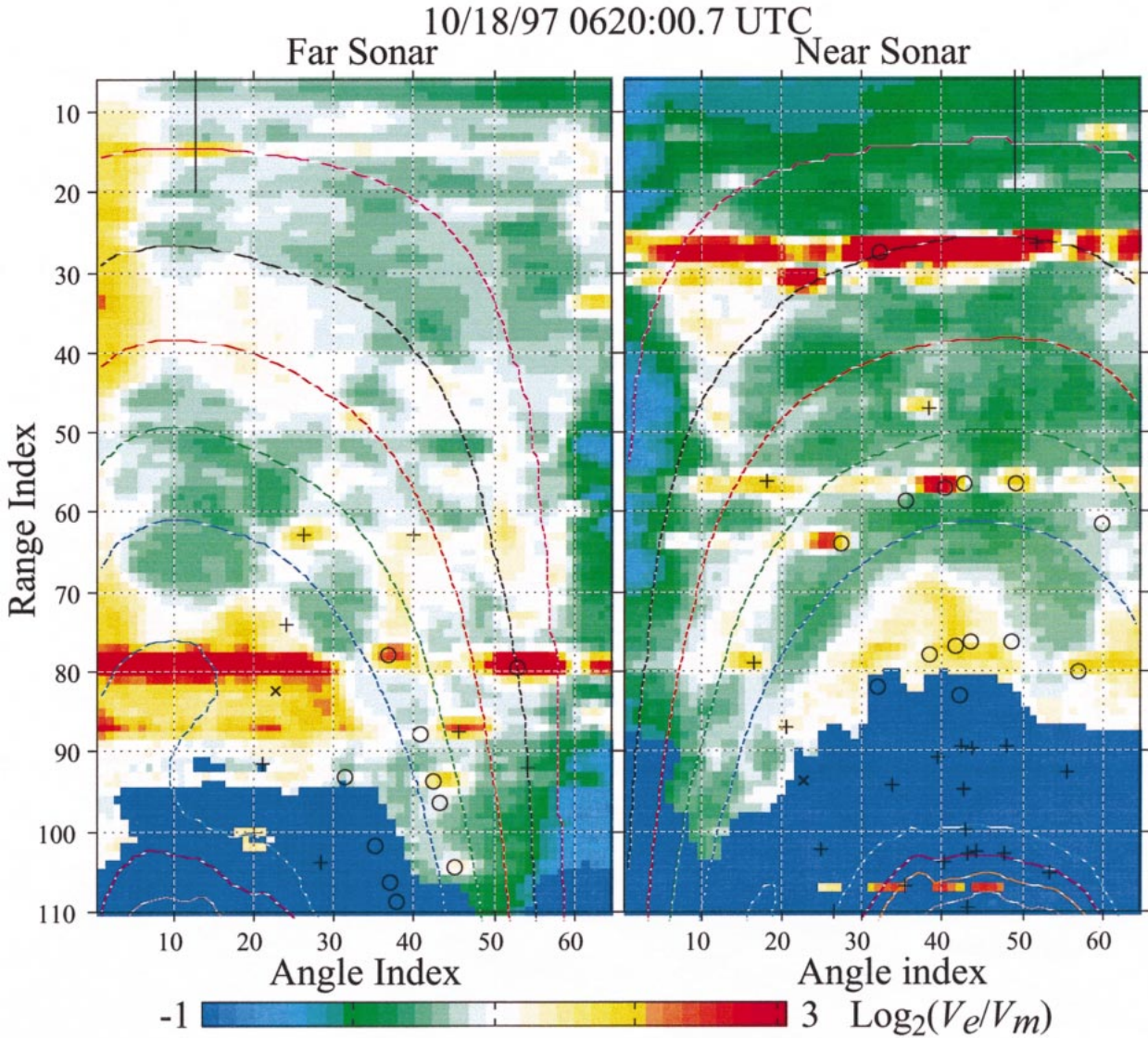


FIG. 5. As in Fig. 4, but for windier conditions, for which there are many scatterers (bubbles) in the water volume. The zero bias (thought to be due to bottom interference) is much smaller in this case.

the principle direction to be angling toward the shoreline. Total horizontal velocity variance is

$$\langle V_T^2 \rangle \equiv \langle V_x^2 \rangle + \langle V_y^2 \rangle, \tag{8}$$

which can be related to the wave height and period via linear theory. In finite depth water, we obtain

$$\langle V_T^2 \rangle = \frac{g^2 k^2 a^2}{\sigma^2} = \left(\frac{gk}{\sigma} \right)^2 \left(\frac{1}{4} H_s \right)^2 = \left(\frac{gkH_s T}{8\pi} \right)^2. \tag{9}$$

The component velocities in coordinates aligned with the wave propagation direction φ are

$$\begin{aligned} V_{\parallel} &= V_x \cos\varphi + V_y \sin\varphi \quad \text{and} \\ V_{\perp} &= V_y \cos\varphi - V_x \sin\varphi, \end{aligned} \tag{10}$$

leading to the wave-aligned variances

$$\begin{aligned} \langle V_{\parallel}^2 \rangle &= \langle V_x^2 \rangle \cos^2\varphi + \langle V_y^2 \rangle \sin^2\varphi \\ &\quad + \langle V_x V_y \rangle \sin 2\varphi \quad \text{and} \end{aligned} \tag{11}$$

$$\begin{aligned} \langle V_{\perp}^2 \rangle &= \langle V_x^2 \rangle \sin^2\varphi + \langle V_y^2 \rangle \cos^2\varphi \\ &\quad - \langle V_x V_y \rangle \sin 2\varphi. \end{aligned} \tag{12}$$

Note that $V_{\parallel}^2 + V_{\perp}^2 = V_T^2$. Also, by construction, the cross correlation between components is zero in these coordinates: $\langle V_{\parallel} V_{\perp} \rangle = 0$. Indeed, if the waves are unidirectional, then $V_{\perp} \equiv 0$. In contrast, if the waves propagate in all directions equally (isotropic), then $V_{\parallel}^2 = V_{\perp}^2 = 1/2 V_T^2$. So, a relevant measure of the directional spread is given by

$$D \equiv \langle V_{\parallel}^2 \rangle / \langle V_T^2 \rangle, \tag{13}$$

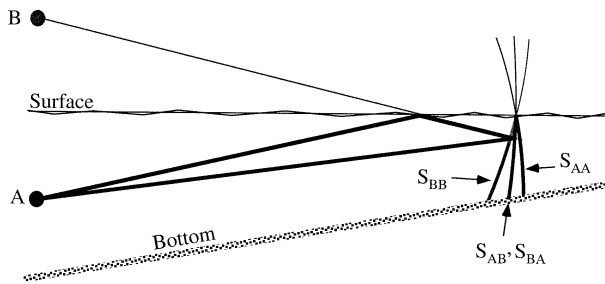


FIG. 6. The surface is a shifting blurry mirror with respect to acoustic propagation. Outgoing and return rays can each take direct or reflected paths, resulting in four routes out and back. For a source/receiver at "A," the image location "B" provides a tool for understanding the paths. The locus of points at a fixed time delay from an impulse transmission has four parts: 1) the direct path out and back yields a spherical segment "S_{AA}" centered on A; 2) the reflected path out and back yields a spherical segment "S_{BB}" centered on B; 3) the reflected path out and direct return "S_{BA}" yields an ellipsoidal segment with foci at A and B; and 4) the direct path out and reflected path back "S_{AB}" yields the same ellipsoidal segment, except that the surface reflection occurs later (on the return trip), by which time the surface may have changed (hence also the net signal phase). Where the segments meet the surface they coincide; at the bottom, the backscattered signal comes from three points (actually, arcs into the page). If the reflection is weak (e.g., absorbed by the bubble layer), the virtual source strength or receive sensitivity at B is adjusted to match. Additional reflections (e.g., off the bottom) make the picture more complex but straightforward: every pair of real or virtual source/receivers forms another ellipsoid. Finite transmission length and averaging thickens the segments into volumes and bottom arcs into areas.

which becomes 1.0 for unidirectional waves and falls to 0.5 for isotropic waves. In general, the results are not sensitive to the value, and D can be set to a value near 0.9 for most nearshore conditions.

These wave-aligned variances provide a simple form for evaluating "radial component" variances (V_R^2), measured along an arbitrary direction θ :

$$\begin{aligned} \langle V_R^2 \rangle &= \langle V_{\parallel}^2 \rangle \cos^2(\varphi - \theta) + \langle V_{\perp}^2 \rangle \sin^2(\varphi - \theta) \\ &= \langle V_{\parallel}^2 \rangle [D \cos^2(\varphi - \theta) + (1 - D) \sin^2(\varphi - \theta)]. \end{aligned} \quad (14)$$

This form appears apt for the PADS data, since the velocity estimates are produced in arrays corresponding to a set of fixed angles by a set of fixed ranges. However, note that the directional spread (and hence D) varies as waves shoal, so this is applicable only with the additional approximation that D does not vary significantly.

A simple but improved approximation can be obtained in beach coordinates, taking advantage of the invariance of k_y . The covariances in beach coordinates can be written

$$\begin{aligned} \langle V_x^2 \rangle &= (g/\sigma)^2 \langle a^2 \rangle \langle k_x^2 \rangle \approx (\text{const}) \langle H_s^2 \rangle \langle k_x^2 \rangle \\ &= (\text{const}) \langle H_s^2 \rangle k^2 \cos^2 \varphi, \end{aligned} \quad (15)$$

$$\langle V_y^2 \rangle = (g/\sigma)^2 \langle a^2 \rangle \langle k_y^2 \rangle = (\text{const}) \langle H_s^2 \rangle, \quad \text{and} \quad (16)$$

$$\begin{aligned} \langle V_x V_y \rangle &= (g/\sigma)^2 \langle a^2 \rangle \langle k_x k_y \rangle \approx (\text{const}) \langle H_s^2 \rangle \langle k_x \rangle \\ &= (\text{const}) \langle H_s^2 \rangle k \cos \varphi. \end{aligned} \quad (17)$$

The approximations in (15) and (17) depend on the variations of k_x being smaller than its mean, $\langle k_x \rangle$. Indeed, the evolution equations for a^2 [(3)] and φ [(6)] implicitly contain similar assumptions. Near shore, this is a good assumption, since the wave direction is generally toward the shore. The results are expressed in terms of quantities for which simple solutions are described above and can be translated back into wave coordinates via (7), (11), (12), and (for D) (13) (see Fig. 3). Using these, (14) provides estimates of radial velocity variances that capture the essential behavior of the waves, as desired. Evolution of the complete frequency-directional spectrum need not be considered in detail.

Figures 4 and 5 illustrate the estimates of rms velocity magnitude due to the incident waves (V_e) divided by that measured (V_m), for the component of velocity along each sonar direction resolved. The ratios are presented as color-contoured maps of $\log_2(V_e/V_m)$ versus range and angle. In calm conditions (Fig. 4), the measured velocities are significantly smaller than those estimated for the incident waves. The discrepancy increases in shallower water. In windy conditions (Fig. 5) the discrepancy is much smaller, with ratios generally smaller than 2 (except very near shore or at the locations of instrumented frames or their sidelobes).

5. Volume versus bottom backscatter

A reasonable hypothesis is that bottom backscatter competes with volume backscatter, biasing the net estimate toward zero. If there were only the direct acoustic path, the bottom backscatter would create a very narrow line at zero Doppler shift, and a line filter could be used to remove it (as is done with some radar systems). However, here paths that include grazing-angle reflections off the surface are also important, introducing small quasi-random Doppler shifts (see Figs. 6, 7). Thus the net bottom backscatter is a statistical variable with an expected Doppler shift of zero and with finite frequency bandwidth. With a little averaging (perhaps as little as 80 ms, or one repeat-sequence-code length; more surely, over a wave period), the bottom backscatter intensity should remain statistically steady over timescales of hours. In contrast, volume backscatter (the signal of primary interest) varies on advection timescales (minutes or faster) or surface wave timescales (seconds), as bubbles are injected and advected. This leads to a simple model to describe, evaluate, and correct for the effect. With this model, the ratio of measured to modeled wave variances (see section 4) can be used to deduce an appropriate division of the averaged backscatter intensity into a "bottom component" and a "volume component."

Exposition of the model requires a brief review of the Doppler processing technique: The Doppler shift is estimated by an autocovariance technique, using repeat sequence codes (Pinkel and Smith 1992). The signal is complex-homodyned to a center frequency of zero, and a time-lagged autocovariance formed. The intensity-

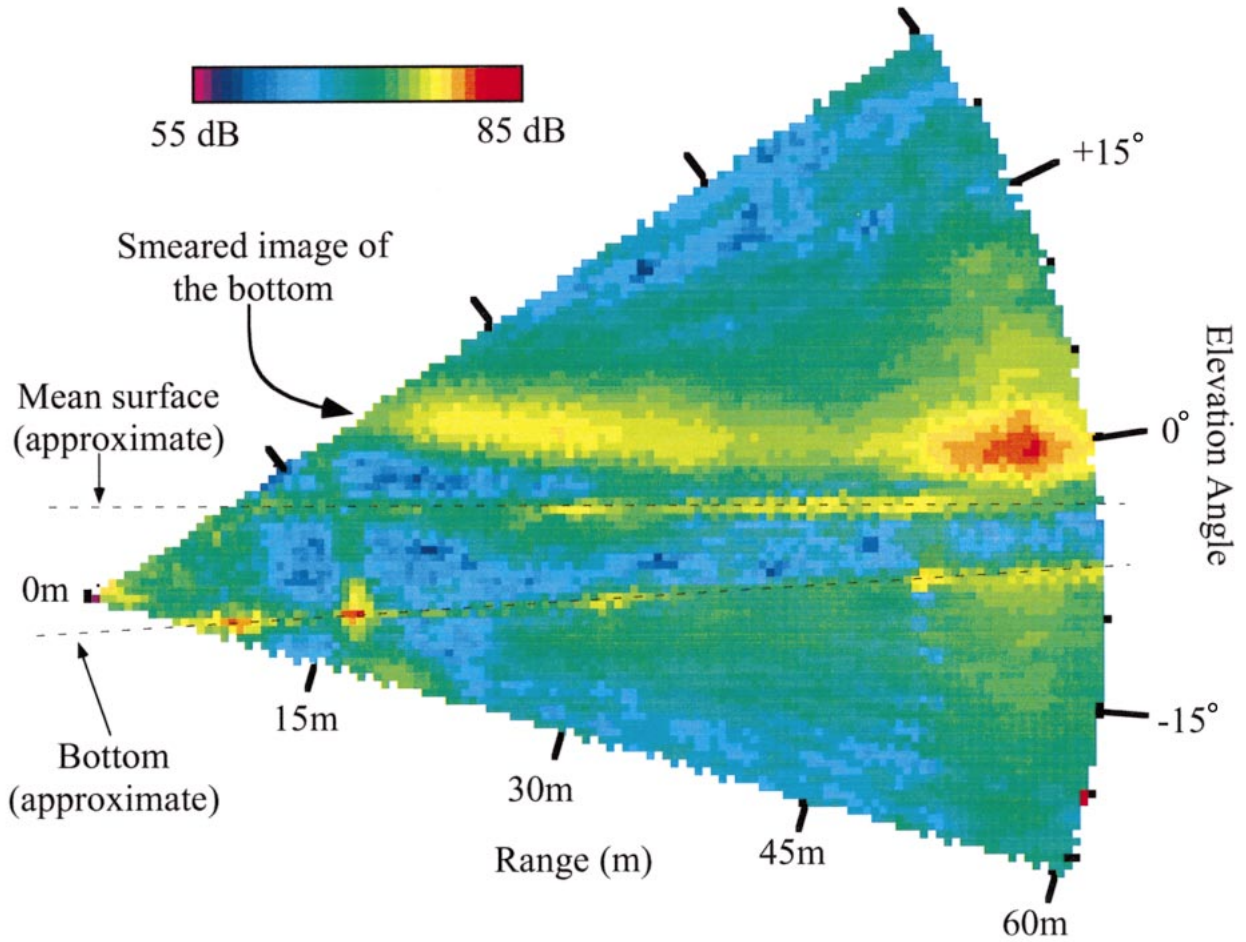


FIG. 7. Intensity plot from a vertical fan beam in shallow water (data taken near Scripps Pier, San Diego, CA, in 1992). The water was unusually clear, because the wind was under 2 m s^{-1} for several days. In addition to a still-visible line of high backscatter from the surface, the bottom and its smeared reflection off the surface are visible in this picture, supporting the interpretation illustrated in Fig. 6. In this picture it appears that the largest integrated return at a fixed range would come from the smeared image of the bottom, reflected off the surface.

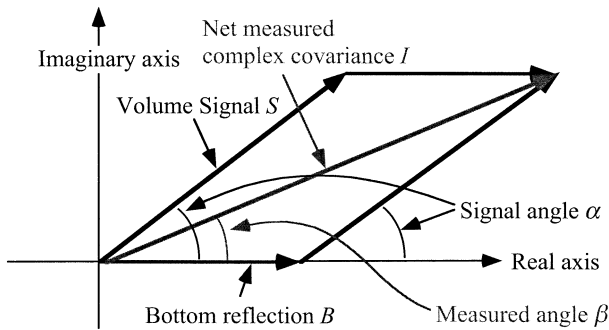


FIG. 8. Illustration of how bottom backscatter contributes to a time-lagged covariance estimate. The addition of a zero-Doppler component B increases the real part of the covariance but leaves the imaginary part unchanged. In general, this biases the estimate to smaller velocities. For small angles (currents much smaller than the ambiguity velocity) and limited bottom backscatter (B not overwhelming S), there is good reason to expect that the effect can be undone. The problem entails five variables: three magnitudes I , B , and S , and the two phase angles, α and β .

weighted mean Doppler shift is proportional to the phase on the complex plane of this autocovariance (Miller and Rochwarger 1972). Figure 8 illustrates the effect of an additive zero-Doppler component and defines the geometry and terminology used here. As illustrated, there are five variables: the desired signal intensity S and its phase α , the bottom intensity B (assumed to have zero phase), and the measured intensity I and its phase β . The real and imaginary parts must separately add up, so there are two equations:

$$I \sin\beta = S \sin\alpha \Rightarrow S = I \left(\frac{\sin\beta}{\sin\alpha} \right) \quad \text{and} \quad (18)$$

$$I \cos\beta = B + S \cos\alpha \Rightarrow B = I \cos\beta - S \cos\alpha = I \left(\cos\beta - \frac{\sin\beta}{\sin\alpha} \right). \quad (19)$$

Solution requires one parameter more than the two mea-

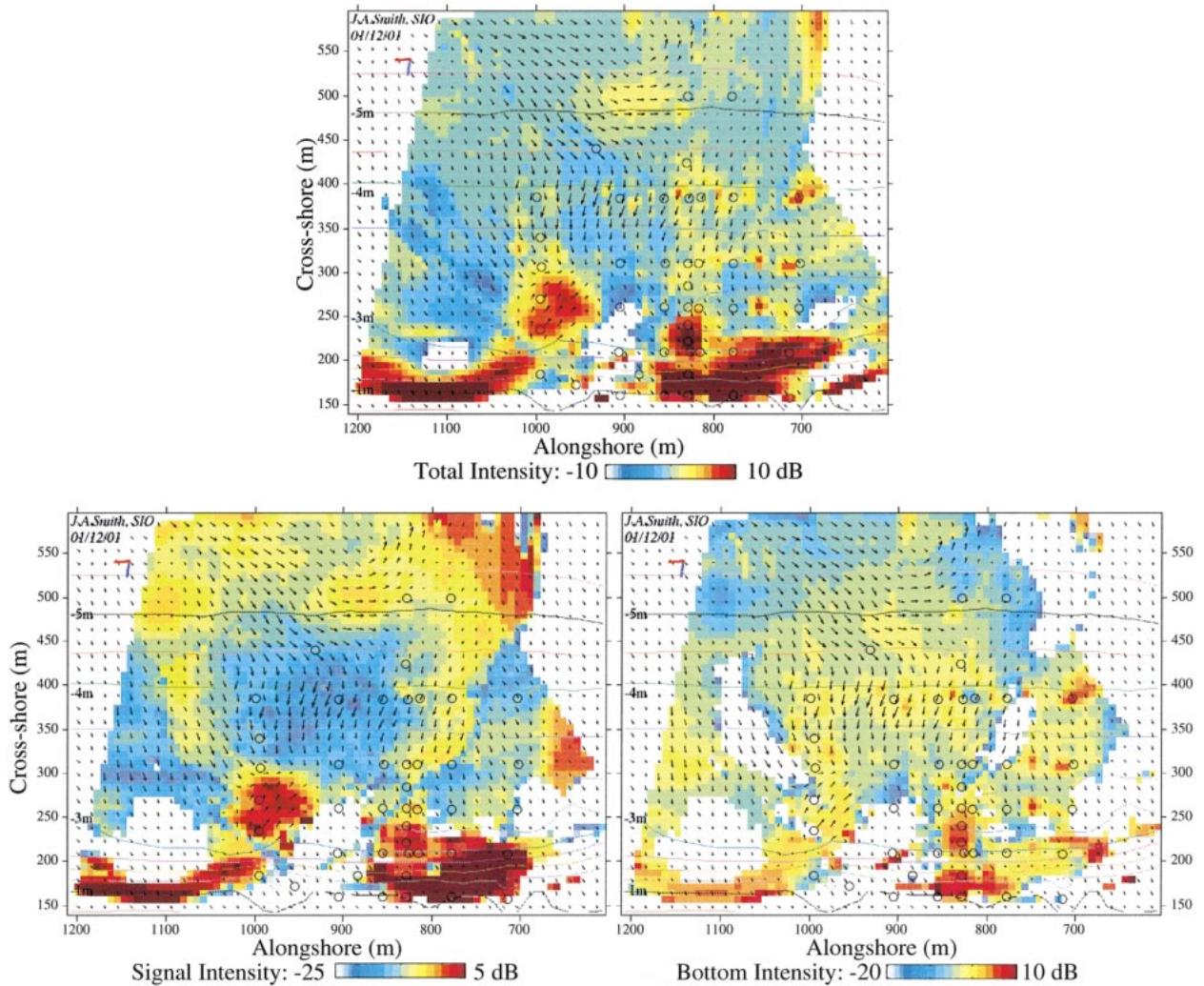


FIG. 9. An example of the separation of the (top) total backscattered acoustic intensity field into the contributions from the (lower left) volume signal and (lower right) bottom backscatter. Note the high-intensity volume fraction advecting out with a rip current near $(x, y) = (1000, 250)$, with little effect on the estimated bottom backscatter relative to the surroundings. Two more patches of higher-backscatter fluid are seen at $(1100, 500)$ and $(900, 500)$; these patches are advecting to the right, parallel to the shore. Arrows represent fluid velocity estimates; an arrow of length equal to the grid spacing corresponds to 40 cm s^{-1} .

sured (I and β). For example, if there were a prior estimate of the bottom backscatter intensity B , an estimate of the signal phase α could be extracted from the measured backscatter parameters I and β :

$$\alpha = \arctan2(I \sin\beta, I \cos\beta - B). \quad (20)$$

Conversely, if there were a prior estimate of α , an estimate of B could be extracted as shown in (19).

The wave model of section 4 provides estimates of wave orbital velocity variances over the fields of view of the sonars. Rigorous use of those here would be difficult; however, for small angles (velocities resulting in covariance phases less than 1 radian or so), the rms values can be rescaled and substituted for the signal phase (from the wave orbital velocity variance maps),

and these can be compared with the measured maps of angular variance. This can only be applied to data averaged over times sufficient to obtain robust variance estimates (say, 2 min or longer). The simple signal model described here provides a way to divide the measured intensity into a component due to bottom backscatter and one due to volume backscatter (both presumably nonnegative; see Fig. 9). The bottom intensities are expected to vary slowly in time, so that rapid variations should appear in the more variable volume component. If so, the model can be inverted, using the measured intensity and a fixed bottom intensity to estimate the volume/bottom backscatter ratio on a ping-by-ping basis. Corrections for the effect can be estimated and applied for every “ping,” improving the response over all

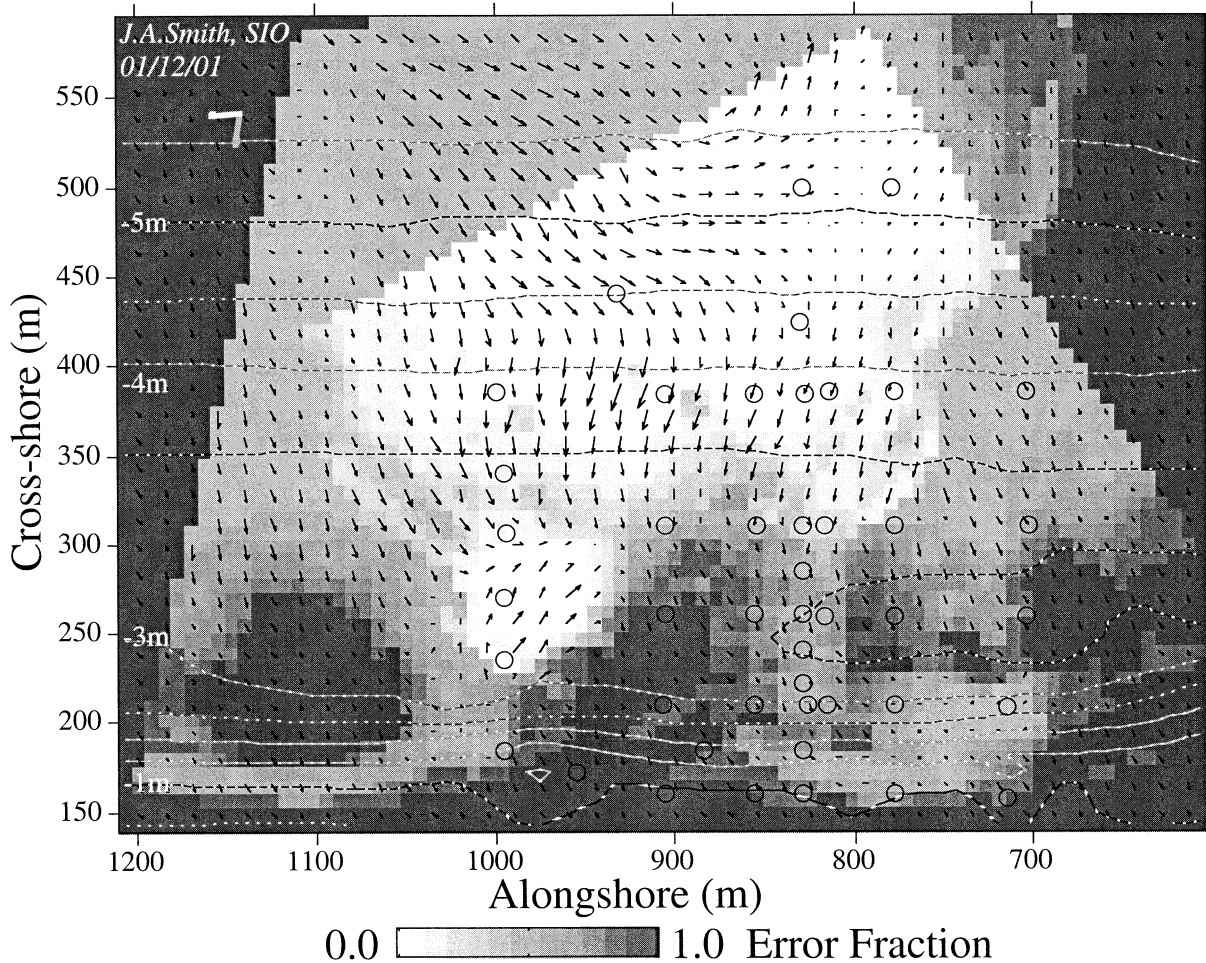


FIG. 10. Velocity vectors with associated error estimates. The fraction of total variance (signal + noise) attributable to error is contoured as shades of gray. For example, if one component of velocity is estimated well and the other is not, this is shaded at the 0.5 level. As in Fig. 9, a vector of length equal to the grid spacing corresponds to an estimated 40 cm s^{-1} fluid velocity.

timescales. The bottom backscatter contribution to the intensity can be verified and updated periodically using time-averaged wave variance estimates.

6. Results and conclusions

Data from discrete locations within the PADS viewing area in SandyDuck were used for direct comparisons of velocity estimates. Near-bottom currents and current profiles in 25-cm vertical bins have been obtained for this purpose. Comparisons between PADS and other current measurements are encouraging, with correlations typically in the range from 0.90 to over 0.99 (depending on the measurements being near-surface or near-bottom and on the existence of stratification).

For lower-frequency motions, such as shear waves and eddies associated with the alongshore shear, the correspondence between near-surface and near-bottom measurements can vary, depending on the stratification. The profile data have been used to evaluate the depth

of the strongest correlation with the PADS data and the correlation with various depth-weighted averages. The depth of measurement most tightly correlated with the PADS estimates is near 1.5 m below the surface (mean with respect to waves, moving with the tide), in line with prior expectations based on experience in deeper water. Where there is strong vertical mixing, currents near the bottom correlate well with the near-surface currents. In contrast, when there is stratification the correlation can become small, with mean angles over 45° between the top and bottom.

A technique was developed here to make the division between bottom and volume backscatter, and so provide corrected estimates of the Doppler shift due to the volume fraction alone in the acoustic signal. The method depends on independent directional wave information, at minimum a mean direction, period, and directional spread. Wave motions, which penetrate in a predictable way to the bottom in finite-depth water, can be compared more readily than lower-frequency motions that may be

baroclinic. At surface-wave frequencies, cross-spectra show high correlations up to frequencies of about 0.2 Hz. Higher-frequency waves have lengths comparable to the 20-m averaging scale of the measurements (i.e., less than 40 m). The wave information could be obtained from the upward sidelobe returns (as suggested by one reviewer), or from an array of pressure sensors on the mounting frame, if the deployment needs to be self-contained.

For the nearly uniform alongshore beach seen seaward of 3-m depth at Duck, a simple wave propagation model can be used to extend the comparison over the whole area probed by each PADS. From this comparison, it is seen that the velocity transfer function varies over time and space. The response is consistent with interference from bottom backscatter (with near-zero Doppler shift) mixing with a highly variable volume backscatter element (e.g., bubble clouds) that advect with the flow. Calibration factors larger than 1 are required to match variances in the surface-wave band from the PADS with those from other instruments, with values generally increasing as the depth decreases (note that correlations remain high, even so). The transfer function variations are large scale and slow as compared with the waves, so (for example) high-resolution frequency-directional spectra are useful, within a global factor to correct the total variance. In particular, phase information is robust (e.g., location and celerity of wave crests), so that wave propagation and refraction can be rigorously examined.

Error estimates on the uncorrected Doppler velocity estimates at finite signal-to-noise estimates are discussed in a companion paper (Smith 2001, manuscript submitted to *J. Atmos. Oceanic Technol.*), based on lower-bound calculations (Theriault 1986) and comparisons with real-world performance of "repeat-sequence" coded pulse systems (Pinkel and Smith 1992). For use in assimilation of the PADS data into a model, the error estimates are simply scaled by the same factor as that applied to the velocity estimates (e.g., see Fig. 10).

Last, note that most previous investigations using sound to probe the nearshore region took place off the West Coast, in particular at Scripps Beach, San Diego, California (Dahl 2001; Farmer et al. 2001; Smith 1993; Smith and Largier 1995; Vagle and Farmer 2001). The steeper bottom slope and lack of sandbars there apparently make bottom interference less of a problem and move the acoustic "bubble barrier" due to breaking surf closer to shore. In this sense, the SandyDuck experiment has proven to be a somewhat more stringent test of the technique than anticipated.

Acknowledgments. This work was supported by ONR Grants N00014-90-J-1285 and N00014-96-1-0030. Thanks are given to S. Elgar (WHOI), R. Guza (SIO), T. Herbers (NPS), and W. O'Reilly (NPS) for providing wave-resolving current meter data from near the bottom at many locations. Thanks are given also to P. Howd

(University of South Florida) for providing 3-min-averaged vertical current profile data at one location. Thanks are also due to R. Pinkel for many good ideas, including the concept of a phased-array sonar, and to E. Slater, M. Goldin, L. Green, C. Neely, J. LeMire, C. Bonner, D. Scarla, and A. Aja for their roles in the design, construction, and deployment of these sonar systems. I also thank W. Birkemeier and the staff of the FRF for their support, help, and enthusiasm during the several months at Duck. Last I thank D. Thompson and A. Berta for help in archiving and analyzing the data.

REFERENCES

- Allen, J. S., P. A. Newberger, and R. A. Holman, 1996: Nonlinear shear instabilities of alongshore currents on plane beaches. *J. Fluid Mech.*, **310**, 181–213.
- Bowen, A. J., and R. A. Holman, 1989: Shear instabilities of the mean longshore current. 1. Theory. *J. Geophys. Res.*, **94**, 18 023–18 030.
- Caruthers, J. W., S. J. Stantic, and P. A. Elmor, 1999: Acoustic attenuation in very shallow water due to the presence of bubbles in rip currents. *J. Acoust. Soc. Amer.*, **106**, 617–625.
- Crawford, C. B., and D. M. Farmer, 1987: On the spatial distribution of ocean bubbles. *J. Geophys. Res.*, **92**, 8231–8243.
- Dahl, P. H., 2001: Bubble clouds and their transport within the surf zone as measured with a distributed array of upward-looking sonars. *J. Acoust. Soc. Amer.*, **109**, 133–142.
- Farmer, D. M., G. B. Deane, and S. Vagle, 2001: The influence of bubble clouds on acoustic propagation in the surf zone. *IEEE J. Oceanic Eng.*, **26**, 113–124.
- Holman, R., 1995: Nearshore processes. *Rev. Geophys.*, **33**, 1237–1247.
- , and A. J. Bowen, 1982: Bars, bumps, and holes: Models for the generation of complex beach topography. *J. Geophys. Res.*, **87**, 457–468.
- Inman, D. L., and B. M. Brush, 1973: The coastal challenge. *Science*, **181**, 20–32.
- , R. J. Tait, and C. E. Nordstrom, 1971: Mixing in the surf zone. *J. Geophys. Res.*, **76**, 3493–3514.
- Kaihatu, J. M., and J. T. Kirby, 1995: Nonlinear transformation of waves in finite water depth. *Phys. Fluids*, **7**, 1903–1914.
- Kennedy, A. B., Q. Chen, J. T. Kirby, and R. A. Dalrymple, 2000: Boussinesq modeling of wave transformation, breaking, end run-up. I: 1D. *J. Waterw., Port, Coastal, Ocean Eng., Amer. Soc. Civil Eng.*, **126**, 39–47.
- Lippmann, T. C., A. H. Brookins, and E. B. Thornton, 1996: Wave energy transformation on natural profiles. *Coastal Eng.*, **27**, 1–20.
- Long, C. E., and J. M. Oltman-Shay, 1991: Directional characteristics of waves in shallow water Tech. U.S. Army Coastal Eng. Res. Center Rep. CERC-91-1, 155 pp.
- Longuet-Higgins, M. S., 1964: Radiation stress in water waves: A physical discussion, with applications. *Deep-Sea Res.*, **11**, 529–562.
- , 1970: Longshore currents generated by obliquely incident sea waves. Parts 1 and 2. *J. Geophys. Res.*, **75**, 6778–6801.
- , and R. W. Stewart, 1962: Radiation stress and mass transport in gravity waves, with application to "surf-beats." *J. Fluid Mech.*, **13**, 481–504.
- Miller, K. S., and M. M. Rochwarger, 1972: A covariance approach to spectral moment estimation. *IEEE Trans. Inf. Theory*, **IT-18**, 588–596.
- Oltman-Shay, J., P. A. Howd, and W. A. Birkemeier, 1989: Shear instabilities of the mean longshore current. 2. Field observations. *J. Geophys. Res.*, **94**, 18 031–18 042.
- Ozkan-Haller, H. T., and J. T. Kirby, 1999: Nonlinear evolution of

- shear instabilities of the longshore current: A comparison of observations and computations. *J. Geophys. Res.*, **104C**, 25 953–25 984.
- Phillips, O. M., 1977: *The Dynamics of the Upper Ocean*. 2d ed. Vol. 1, *Cambridge Monographs on Mechanics and Applied Mathematics*, Cambridge University Press, 336 pp.
- Pinkel, R., and J. A. Smith, 1992: Repeat-sequence coding for improved precision of Doppler sonar and sodar. *J. Atmos. Oceanic Technol.*, **9**, 149–163.
- Raubenheimer, B., R. T. Guza, and S. Elgar, 1996: Wave transformation across the inner surf zone. *J. Geophys. Res.*, **101**, 25 589–25 597.
- Reniers, A. J. H. M., J. A. Battjes, A. Falques, and D. A. Huntley, 1997: A laboratory study on the shear instability of longshore currents. *J. Geophys. Res.*, **102**, 8597–8609.
- Shepard, F. P., and D. L. Inman, 1950: Nearshore water circulation related to bottom topography and wave refraction. *Trans. Amer. Geophys. Union*, **31**, 196–212.
- Slinn, D. N., J. S. Allen, P. A. Newberger, and R. A. Holman, 1998: Nonlinear shear instabilities of alongshore currents over barred beaches. *J. Geophys. Res.*, **103C**, 18 357–18 379.
- Smith, J. A., 1993: Performance of a horizontally scanning Doppler sonar near shore. *J. Atmos. Oceanic Technol.*, **10**, 752–763.
- , 1998: Evolution of Langmuir circulation during a storm. *J. Geophys. Res.*, **103**, 12 649–12 668.
- , 2001: Continuous time–space sampling of surface currents using sound. *J. Atmos. Oceanic Technol.*, submitted.
- , and J. L. Largier, 1995: Observations of nearshore circulation—Rip currents. *J. Geophys. Res.*, **100**, 10 967–10 975.
- Theriault, K. B., 1986: Incoherent multibeam Doppler current profiler performance. Part I: Estimate variance. *J. Ocean Eng.*, **OE-11**, 7–15.
- Thornton, E. B., and R. T. Guza, 1986: Surf zone longshore currents and random waves: Field data and models. *J. Phys. Oceanogr.*, **16**, 1165–1178.
- Thorpe, S. A., 1986: Bubble clouds: A review of their detection by sonar, of related models, and of how K_r may be determined. *Oceanic Whitecaps and Their Role in Air–Sea Exchange Processes*, E. C. Monahan and G. MacNiocaill, Eds., D. Reidel, 57–68.
- , and A. J. Hall, 1993: Nearshore side-scan sonar studies. *J. Atmos. Oceanic Technol.*, **10**, 778–783.
- Vagle, S., and D. M. Farmer, 2001: Bubble transport in rip currents. *J. Geophys. Res.*, **107C**, 11 677–11 689.
- Whitham, G. B., 1974: *Linear and Nonlinear Waves*. Wiley-Interscience, 636 pp.